Available online at www.sciencedirect.com
SCIENCE DIRECT®
Physica C 426–431 (2005) 1552–1560
PHYSICA C
www.elsevier.com/locate/physc

Coherent manipulation of coupled Josephson charge qubits

Yu.A. Pashkin [a,b,*,1], T. Yamamoto [a,b], O. Astafiev [a], Y. Nakamura [a,b], D.V. Averin [c], T. Tilma [a,d], F. Nori [a,d], J.S. Tsai [a,b]

[a] The Institute of Physical and Chemical Research (RIKEN), Wako, Saitama 351-0198, Japan
[b] NEC Fundamental Research Laboratories, 34 Miyukigaoka, Tsukuba, Ibaraki 305-8501, Japan
[c] Department of Physics and Astronomy, SUNY at Stony Brook, Stony Brook, NY 11794-3800, USA
[d] Department of Physics, University of Michigan, Ann Arbor, MI 48109-1120, USA

Received 23 November 2004; accepted 4 January 2005
Available online 19 July 2005

Abstract

We have analyzed and measured the quantum coherent dynamics of a circuit containing two-coupled superconducting charge qubits. Each qubit is based on a Cooper pair box connected to a reservoir electrode through a Josephson junction. Two qubits are coupled electrostatically by a small island overlapping both Cooper pair boxes. Quantum state manipulation of the qubit circuit is done by applying non-adiabatic voltage pulses to the common gate. We read out each qubit by means of probe electrodes connected to Cooper pair boxes through high-Ohmic tunnel junctions. With such a setup, the measured pulse-induced probe currents are proportional to the probability for each qubit to have an extra Cooper pair after the manipulation. As expected from theory and observed experimentally, the measured pulse-induced current in each probe has two frequency components whose position on the frequency axis can be externally controlled. This is a result of the inter-qubit coupling which is also responsible for the avoided level crossing that we observed in the qubits' spectra. Our simulations show that in the absence of decoherence and with a rectangular pulse shape, the system remains entangled most of the time reaching maximally entangled states at certain instances.

PACS: 03.67.Lx; 74.50.+r; 85.25.C

Keywords: Quantum computing; Solid-state qubits; Quantum coherence; Entanglement

1. Introduction

From starting as a purely mathematical discipline a few years ago, quantum computation has turned into an experimental subject, recently

* Corresponding author. Address: NEC Fundamental Research Laboratories, 34 Miyukigaoka, Tsukuba, Ibaraki 305-8501, Japan. Tel.: +81 029 850 2602; fax: +81 029 850 2624.
E-mail address: pashkin@frl.cl.nec.co.jp (Yu.A. Pashkin).
[1] On leave from Lebedev Physical Institute, Leninskii Prospekt 53, Moscow 119991, Russia.

0921-4534/$ - see front matter © 2005 Elsevier B.V. All rights reserved.
doi:10.1016/j.physc.2005.01.076

attracting the efforts of experimentalists from various fields [1,2]. One of the main goals of experimentalists now is to find a proper physical system that can be used as a quantum bit (qubit), a building block of a quantum computer. Although quite many physical systems have been suggested as potential implementations of qubits, solid-state systems, and superconducting systems in particular [3,4], are of great interest because they offer the possibility of scaling to a large number of interacting qubits. Within the past few years, there has been substantial experimental progress with single solid-state qubits in which coherent manipulation of quantum states has been performed [5–11]. Superconducting qubits utilize charge [5–7] or flux [8] degrees of freedom, or energy levels quantization in a single Josephson junction [9,10]. Charge qubits are based on a Cooper pair box whose state is read-out by means of a probe junction [5], the switching of a large Josephson junction [6], or a sensitive fast electrometer, e.g., radio-frequency single-electron transistor (SET) [7], or a charge trap coupled to a conventional SET [12].

One of the key steps in constructing a quantum computer is to couple two qubits and then scale the circuit to many qubits. Despite substantial progress in single qubit operation, there has been very little work done to couple several solid-state qubits. Measurements in the time domain have been performed on two-coupled charge qubits [13]. Spectroscopic measurements have been carried out on coupled single junction [14] and flux qubits [15].

Here, we summarize our experiment on two-coupled superconducting charge qubits [13] adding more experimental details and presenting analytical expressions for the time evolution of the probability amplitudes and entropy of entanglement for the case of a rectangular pulse shape in the absence of decoherence.

2. Two-qubit circuit diagram

One of the physical realizations of a solid-state qubit is provided by a Cooper pair box [16,17] which is a small superconducting island connected to a large superconducting electrode, a reservoir, through a Josephson junction. The two charge states of the box, say $|0\rangle$ and $|1\rangle$, differing by one Cooper pair, are coherently mixed by the Josephson coupling as was confirmed experimentally [18]. Quantum state manipulation of such a system can be done by using a non-adiabatic pulse technique, and the read-out can be performed by a properly biased probe electrode [5]. Here, we take two charge qubits and couple them by means of a miniature on-chip capacitor. The read-out of each qubit, in this case, is done similar to the single-qubit read-out: we connect a probe electrode to each qubit. We then perform state manipulation and demonstrate qubit–qubit interaction.

The circuit we study is shown schematically in Fig. 1. It is made of aluminum by angle evaporation through a suspended mask prepared by electron-beam lithography and dry etching. Exposing the Al surfaces to oxygen in the evaporation chamber after each evaporation step forms the tunnel junctions. The oxidation parameters (oxidation time and gas pressure) were different for Josephson and probe tunnel junctions. The measurements are done in a dilution refrigerator with a mixing chamber temperature of about 40 mK.

The circuit consists of two charge qubits that are electrostatically coupled by an on-chip capacitor C_m. The right qubit has a SQUID geometry to allow for the control of the Josephson coupling to its reservoir while the Josephson coupling of the left qubit is fixed. Both qubits have a common pulse gate but separate dc gates, probes and reservoirs. The pulse gate has nominally equal coupling to each box. In the experiment, both reservoirs are

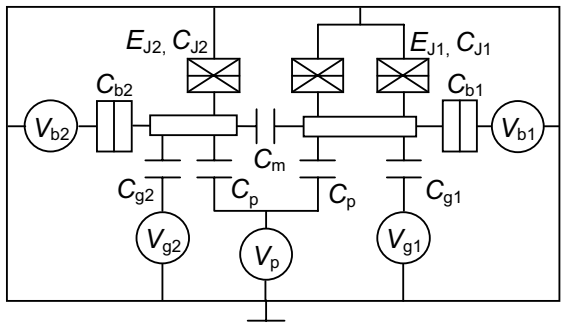

Fig. 1. Schematic diagram of the two-coupled-qubit circuit. Black bars denote Cooper pair boxes.

kept grounded. External controls that we have in the circuit are the dc probe voltages V_{b1} and V_{b2}, dc gate voltages V_{g1} and V_{g2}, and pulse gate voltage V_p. The information on the final states of the qubits after manipulation comes from the pulse-induced currents measured in the probes. An interesting feature of the circuit is that all its essential parameters (e.g., charging energies and Josephson energies) can be obtained from various independent measurements. For example, each qubit can be measured as a single-electron transistor in the dc regime. The current between reservoir and probe in each SET depends on the dc voltages applied to probes and dc gates. By doing routine current–voltage–gate voltage measurements, we can estimate the capacitances indicated in Fig. 1: $C_{J1} = 620$ aF, $C_{J2} = 460$ aF, $C_{b1} = 41$ aF, $C_{b2} = 50$ aF, $C_{g1} = 0.60$ aF, $C_{g2} = 0.61$ aF, $C_p \approx 1$ aF, $C_m = 34$ aF. These give the following values of the characteristic energies: Cooper pair charging energy of the first (right in Fig. 1) qubit $E_{c1} = 484$ μeV (117 GHz in frequency units), Cooper pair charging energy of the second (left in Fig. 1) qubit $E_{c2} = 628$ μeV (152 GHz) and the coupling energy $E_m = 65$ μeV (15.7 GHz). All these energies are higher than the energy of thermal fluctuations $k_B T \sim 3$ μeV (0.7 GHz). The charging and the coupling energies are defined as follows: $E_{c1,2} = 4e^2 C_{\Sigma 2,1}/2(C_{\Sigma 1}C_{\Sigma 2} - C_m^2)$, where $C_{\Sigma 1,2}$ are the sum of all capacitances connected to the corresponding Cooper pair box including the coupling capacitance C_m, and $E_m = 4e^2 C_m/(C_{\Sigma 1}C_{\Sigma 2} - C_m^2)$. Here, e is the electron charge. The way we determine the qubits' Josephson energies E_{J1} and E_{J2} will be described later in the text.

3. Two-qubit circuit model

The Hamiltonian of the system in the charge representation can be written as

$$\begin{aligned} H = \sum_{n_1,n_2} \Big[& E_{c1}(n_{g1} - n_1)^2 + E_{c2}(n_{g2} - n_2)^2 \\ & + E_m(n_{g1} - n_1)(n_{g2} - n_2) \Big] |n_1 n_2\rangle\langle n_1 n_2| \\ & - \frac{E_{J1}}{2} [|n_1 n_2\rangle\langle (n_1+1) n_2| \\ & + |n_1 (n_2+1)\rangle\langle (n_1+1)(n_2+1)|] \\ & - \frac{E_{J2}}{2} [|n_1 n_2\rangle\langle n_1 (n_2+1)| \\ & + |(n_1+1) n_2\rangle\langle (n_1+1)(n_2+1)|]. \end{aligned} \quad (1)$$

Here, n_1 and n_2 ($n_1, n_2 = 0, \pm 1, \pm 2, \ldots$) are the numbers of excess Cooper pairs in the first and the second Cooper pair boxes, and $n_{g1,2} = (C_{g1,2}V_{g1,2} + C_p V_p)/2e$ are the normalized charges induced on the corresponding qubit by the dc and pulse gate electrodes. The eigenenergies, E_k ($k = 0, 1, 2, \ldots$), of the Hamiltonian (1) form 2e-periodic energy bands corresponding to the ground ($k = 0$), first excited ($k = 1$), etc. states of the system. The energy bands E_k for the one-dimensional case were first introduced in Ref. [19]. A contour plot of the ground energy band around zero gate-induced charge is shown in Fig. 2. It consists of hexagonal cells (shown partly) whose boundaries marked by the dashed lines delimit two neighboring charge states with equal electrostatic energies. For example, points R and L correspond to degeneracies between the states $|00\rangle$ and $|10\rangle$, and the states $|00\rangle$ and $|01\rangle$ that differ by one Cooper pair in the first (right) and the second (left) Cooper pair box, respectively. The band has minimums in the

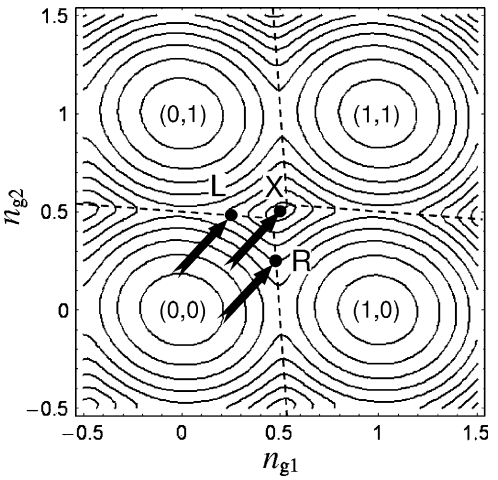

Fig. 2. Contour plot of the ground state energy band as a function of the normalized gate charges n_{g1} and n_{g2}. Dashed lines are boundaries between charge states (n_1, n_2) differing by one Cooper pair. The three thick arrows indicate non-adiabatic pulse shifts of the system from the initial states within the cell (00).

middle of each cell and also maximums in between (one of the maximums is marked by X). If we choose the dc gate charges n_{g1} and n_{g2} far from the boundaries but within the $(0,0)$ cell, then because of the large electrostatic energies we can assume that the system remains in the state $|00\rangle$. Strictly speaking, this charge stability diagram [20] is valid in the absence of Josephson coupling; however, it also remains valid for small Josephson coupling, except at the boundaries where the charge states become superposed. Since the pulse gate has equal coupling to each qubit, the application of a pulse shifts the state of the system on this diagram along the line tilted at 45° (indicated by arrows in Fig. 2). The dynamics of the system strongly depends on how fast it is driven by the gate voltages and on the final point it is driven to. If only dc gate voltages are applied, then the system stays in the ground energy band, but can be moved from one cell to another. If a pulse voltage is applied, then excited energy bands become involved. When the system is driven non-adiabatically to the point R or L, it behaves like a single qubit oscillating between the degenerate states with a frequency $\omega_{1,2} = E_{J1,2}/\hbar$. Let us first consider the cross-section of the energy bands through the point R along the pulse direction shown by the arrow pointing at R in Fig. 2. The cross-section is presented in Fig. 3a. The four eigenenergies are grouped in two pairs, and each pair has its own degeneracy ($E_{00} = E_{10}$, $E_{01} = E_{11}$) shifted with respect to each other by an amount determined by the coupling energy E_m and separated by a large energy gap from other states. If the system is prepared in the $|00\rangle$ initial state and then pulse-driven to the point R, the system starts to evolve quantum coherently between only two states: $|00\rangle$ and $|10\rangle$. To describe the dynamics of the system around the point R, we can consider only these two states as a basis. The Hamiltonian of the system in this case is a 2×2 matrix with electrostatic energies E_{00} and E_{10} as diagonal elements and $-E_{J1}/2$ as off-diagonal elements. The probability to be in the state $|10\rangle$ oscillates as $(1-\cos\omega_1 t)/2$. This corresponds to the single (first) qubit oscillation while the number of Cooper pairs in the second qubit remains constant (zero). In other words, we have coherent oscillations in the first qubit while the second one

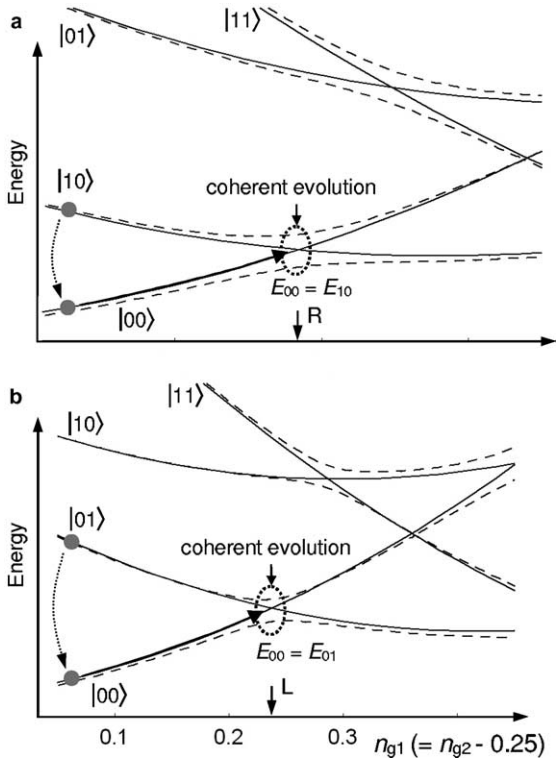

Fig. 3. Cross-sections of energy bands through points R and L in Fig. 2. Dashed lines: eigenenergies of the Hamiltonian (2) showing only the four lower states. Solid lines: electrostatic energies E_{00}, E_{10}, E_{01}, and E_{11}. Solid arrows along E_{00} indicate pulse drives. Quantum state evolution takes place at the gate voltages corresponding to the lower degeneracy point $E_{00} = E_{10}$ (a) or $E_{00} = E_{01}$ (b). The two upper states are not involved. Dotted lines on the left show the decay of the excited state ($|10\rangle$ or $|01\rangle$) after the evolution (termination of the pulse). This decay gives rise to the pulse-induced dc probe current in the first or second probe.

remains in the blockade regime. Similar oscillations in the second qubit will take place when the system is driven to the point L. The corresponding cross-section of the energy diagram is shown in Fig. 3b. The lower degeneracy is between states $|00\rangle$ and $|01\rangle$. In this case, the first qubit remains in the blockade regime while the second one oscillates coherently with the probability of state $|01\rangle$ being equal to $(1-\cos\omega_2 t)/2$). Applying arrays of pulses and measuring oscillations of the probe currents I_1 and I_2, we can determine the Josephson energies of each qubit. The accuracy of the

measured $E_{J1,2}$ is very high since the electrostatic coupling through C_m has almost no effect on $\omega_{1,2}$ along the boundaries in the vicinity of R and L. The corresponding experimental data is shown in Fig. 5.

Now let us consider point X in Fig. 2 which is a peak in the ground energy band. This point corresponds to two degeneracies: $E_{00} = E_{11}$ and $E_{10} = E_{01}$, therefore we call this a double-degeneracy point. If the circuit is fabricated to have the following relation between the characteristic energies: $E_{J1,2} \sim E_m < E_{c1,2}$, then we can use a four-level approximation for the description of the system. The state of the system in the vicinity of X can be described by the coherent superposition of the four charge states $|00\rangle$, $|01\rangle$, $|10\rangle$ and $|11\rangle$ around $n_{g1} = n_{g2} = 0.5$ while other charge states are separated by large energy gaps. These four charge states can be used as a new basis and the Hamiltonian (1) can be simplified to the following 4×4 matrix form:

$$H = \begin{bmatrix} E_{00} & -\frac{1}{2}E_{J1} & -\frac{1}{2}E_{J2} & 0 \\ -\frac{1}{2}E_{J1} & E_{10} & 0 & -\frac{1}{2}E_{J2} \\ -\frac{1}{2}E_{J2} & 0 & E_{01} & -\frac{1}{2}E_{J1} \\ 0 & -\frac{1}{2}E_{J2} & -\frac{1}{2}E_{J1} & E_{11} \end{bmatrix}, \qquad (2)$$

where $E_{n1n2} = E_{c1}(n_{g1} - n_1)^2 + E_{c2}(n_{g2} - n_2)^2 + E_m(n_{g1} - n_1)(n_{g2} - n_2)$ is the total electrostatic energy of the system $(n_1, n_2 = 0, 1)$. The cross-section of the energy bands through the point X is presented in Fig. 4. Here, the dynamics of the quantum evolution becomes more complex (involving all for charge states) and reflects the coupling between the qubits. Exactly at the double-degeneracy point, the time evolution of the system can be described analytically for any initial state. First, we write down the state of the system in general as

$$|\psi(t)\rangle = c_1|00\rangle + c_2|10\rangle + c_3|01\rangle + c_4|11\rangle, \qquad (3)$$

where $|c_i|$ $(i = 1, 2, 3, 4)$ are the time dependent probability amplitudes obeying the normalization condition $\sum_{i=1}^{4}|c_i|^2 = 1$. Then, we use Hamiltonian (2) and the initial state $|00\rangle$ and obtain the following dependence of the probability amplitudes on time:

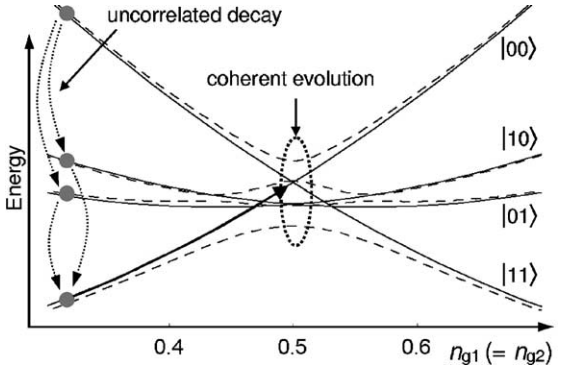

Fig. 4. Cross-section of energy bands through the point X in Fig. 2. Dashed lines: eigenenergies of Hamiltonian (2). Solid lines: electrostatic energies E_{00}, E_{10}, E_{01}, and E_{11}. Solid arrow along E_{00} indicates non-adiabatic pulse shift of the system. Quantum state evolution involving all four basis states takes place at the gate voltages $n_{g1} = n_{g2} = 0.5$ corresponding to the double-degeneracy point X in Fig. 2: $E_{00} = E_{11}$ and $E_{10} = E_{01}$. Dotted lines on the left show qualitatively the decay of the excited states ($|11\rangle$, $|10\rangle$ and $|01\rangle$) after the evolution (termination of the pulse). This decay gives rise to the pulse-induced probe currents in both probes.

$$\begin{aligned} c_1 &= \frac{1}{2}[\cos\Omega t + \cos\varepsilon t] - \frac{iE_m}{8\hbar\Omega\varepsilon}[\varepsilon\sin\Omega t + \Omega\sin\varepsilon t], \\ c_2 &= \frac{i}{4}\left[\frac{E_{J1}+E_{J2}}{\hbar\Omega}\sin\Omega t + \frac{E_{J2}-E_{J1}}{\hbar\varepsilon}\sin\varepsilon t\right], \\ c_3 &= \frac{i}{4}\left[\frac{E_{J1}+E_{J2}}{\hbar\Omega}\sin\Omega t - \frac{E_{J2}-E_{J1}}{\hbar\varepsilon}\sin\varepsilon t\right], \\ c_4 &= \frac{1}{2}[\cos\Omega t - \cos\varepsilon t] - \frac{iE_m}{8\hbar\Omega\varepsilon}[\varepsilon\sin\Omega t - \Omega\sin\varepsilon t], \end{aligned} \qquad (4)$$

where $\Omega = ((E_{J1} + E_{J2})^2 + (E_m/2)^2)^{1/2}/2\hbar$, $\varepsilon = ((E_{J1} - E_{J2})^2 + (E_m/2)^2)^{1/2}/2\hbar$.

Similar expressions for the time evolution of amplitudes can be obtained for the other initial states. Preparation of excited initial states $|10\rangle$, $|01\rangle$ and $|11\rangle$ requires a different pulsing part of the circuit: we would need separate pulse gates for each qubit in order to address each qubit individually and flip them. This was done in our later experiment [21], with a two-qubit circuit where two pulse gates were utilized. In the present work, we use one common pulse gate and assume state $|00\rangle$ as an initial state.

From the expressions (4), we can calculate observable quantities, e.g., probabilities $|c_i|^2$ of each charge state. However, in our read-out scheme, we measure a probe current $I_{1,2}$ proportional to the probability $p_{1,2}(1)$ for each qubit to have a Cooper pair on it, regardless of the state of the other qubit, i.e., $I_1 \propto p_1(1) \equiv |c_2|^2 + |c_4|^2$ and $I_2 \propto p_2(1) \equiv |c_3|^2 + |c_4|^2$. Assuming the initial state at $t = 0$ is $|00\rangle$, we can derive for an ideal rectangular pulse shape of a length t the time evolution of these probabilities:

$$p_{1,2}(1) = (1/4)\big[2 - (1 - \chi_{1,2})\cos\{(\Omega + \varepsilon)t\} - \big(1 + \chi_{1,2}\big)\cos\{(\Omega - \varepsilon)t\}\big], \quad (5)$$

where $\chi_{1,2} = (E_{J2,1}^2 - E_{J1,2}^2 + E_m^2/4)/(4\hbar^2\Omega\varepsilon)$.

One can see that unlike single qubit case, there are two frequencies present in the oscillation spectrum of the qubits: $\Omega + \varepsilon$ and $\Omega - \varepsilon$, both dependent on E_{J1}, E_{J2} and E_m. Note that in the uncoupled situation ($E_m = 0$), $\Omega \pm \varepsilon = E_{J1,2}/\hbar$ each qubit oscillates with its own frequency $\omega_{1,2}$. Let us stress, however, that the above treatment is valid only in the ideal case when the pulse has zero rise/fall time and the time evolution occurs exactly at the double-degeneracy point.

4. Experimental results

The idea of the experiment is shown schematically in Fig. 2. First, to determine E_{J1} and E_{J2}, we bring the system to the points R or L from the initial state $|00\rangle$ (within the cell (00)). The initial state is adjusted by the dc gate voltages, and the pulse voltages are shown schematically by thick black arrows. In this case the system oscillates as a single qubit (first or second) as described earlier in the text. The final states are measured as probe currents resulting from the decay of the excited states ($|10\rangle$ or $|01\rangle$). Thus, coherent Cooper pair tunneling through Josephson junction and incoherent decay of the final state as two quasiparticle tunneling events through the probe junction are the two steps of the so-called Josephson-quasiparticle cycle [22]. The current from the single manipulation event, $\sim 2e/\tau_m \sim 10^{-17}$ A (where $\tau_m = 20$ ms is the measurement time), appears too low to be measured by any existing current meters. Therefore, to accumulate a signal, we apply a pulse array ($\sim 3 \times 10^5$ pulses) to the pulse gate. The estimated amplitude of the applied pulses is $V_p \approx 30$ mV. The repetition time between the pulses is 64 ns, long enough (in comparison to the quasiparticle relaxation time $\sim$10 ns) to let the system relax to the ground state through a quasiparticle decay and to give rise to a probe current proportional to $p_{1,2}$. The expected current oscillation amplitude is $2e$/repetition time = 5 pA. The corresponding oscillations of the probe currents I_1 and I_2 are shown in Fig. 5. The observed amplitudes are 2.5 pA for the first qubit and 3.5 pA for the second one. This gives the qubit efficiency of 50% and 70%, respectively. Note, however, that these amplitudes were estimated at $t = 80$ ps, the minimum pulse length provided by our pulse pattern generator. The oscillations can be fitted to a cosine function with an exponential decay time of about 2.5 ns. The oscillations spectra (right panels of Fig. 5) obtained by Fourier transform contains one pronounced component at 13.4 GHz for the first qubit and another at 9.1 GHz for the second one. We identify these values with E_{J1} and E_{J2}. Judging from our previous experiments

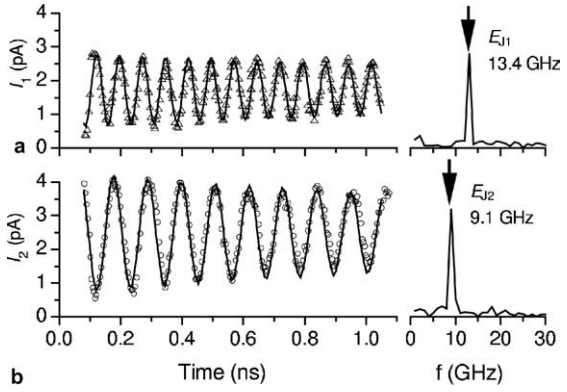

Fig. 5. Probe current oscillations in the first (a) and the second (b) qubit when the system is driven non-adiabatically to the points R and L, respectively. Right panels show the corresponding spectra obtained by the Fourier transform. Peak position in the spectrum gives the value of the Josephson energy of each qubit, indicated by arrow. In both cases, the experimental data (open triangles and open dots) can be fitted to a cosine dependence (solid lines) with an exponential decay with 2.5 ns time constant.

we can conclude that these values are close to what we expect for the given fabrication parameters, i.e., overlap area and oxidation conditions.

Next, we repeat the same procedure shifting the system to the point X by an array of pulses and measuring again the oscillations of the pulse-induced currents I_1 and I_2. The pulse (solid arrow in Fig. 4) brings the system to the double-degeneracy point, and the system evolves for the pulse duration time t, producing a superposed state (3). After the pulse terminates, the system remains in the superposed state until it decays (dotted arrows in Fig. 4) to the ground state by emitting quasiparticles into the probe junctions biased at $V_{b1,2} \approx 600$ μeV.

The results obtained in this way are presented in Fig. 6. The oscillation pattern becomes more complex and more frequency components appear in the spectrum (right panels in Fig. 6). The observed spectral properties of the oscillations agree with the predictions of Eq. (5) in a sense that there are two peaks in the spectrum and the peak positions are close to the expected frequencies $\Omega + \varepsilon$ and $\Omega - \varepsilon$ for the parameters $E_{J1} = 13.4$ GHz and $E_{J2} = 9.1$ GHz measured in the single qubit experiments (Fig. 5), and $E_m = 15.7$ GHz estimated from the independent dc current–voltage characteristics measurements. Positions of the $\Omega + \varepsilon$ and $\Omega - \varepsilon$ peaks expected from Eq. (6), are indicated by arrows and dotted lines. The decay time ~0.6 ns of the coupled oscillations is shorter when compared to the case of independent oscillations as should be expected since qualitatively an extra decoherence channel appears for each qubit after coupling to its neighbor (see quantitative discussion in Ref. [23]). The amplitudes of the spectral peaks, however, do not exactly agree with Eq. (6). We attribute this to the non-ideal pulse shape (finite rise/fall time ~35 ps), and the fact that a small shift of n_{g1} and n_{g2} from the double-degeneracy point drastically changes the oscillation pattern. Also, even far from the double degeneracy, we still have a small contribution to the initial state from the other charge states which distorts the oscillations. We found that $E_m = 14.5$ GHz, close to the value estimated from the dc measurements, gives better agreement of the fit with the experimental data.

Finally, we checked the dependence of the oscillation frequencies on E_{J1} controlled by a weak magnetic field (up to 20 Gs). The results are shown in Fig. 7. The plot contains the data from both qubits represented by open triangles (first qubit) and open circles (second qubit). Without coupling

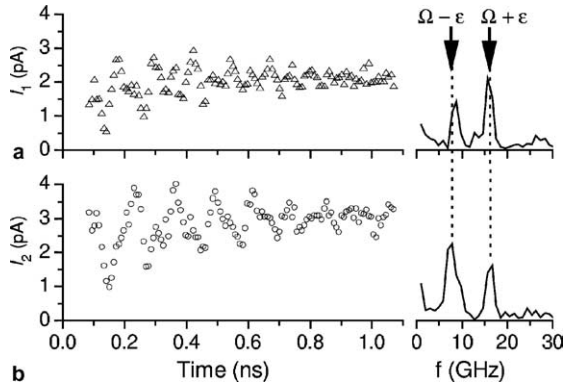

Fig. 6. Probe current oscillations in the first (a) and the second (b) qubit when the system is driven non-adiabatically to the double-degeneracy point X for the case $E_{J1} = 9.1$ GHz and $E_{J2} = 13.4$ GHz. Right panels show the corresponding spectra obtained by Fourier transformation. Arrows and dotted lines indicate theoretically expected position of the peaks.

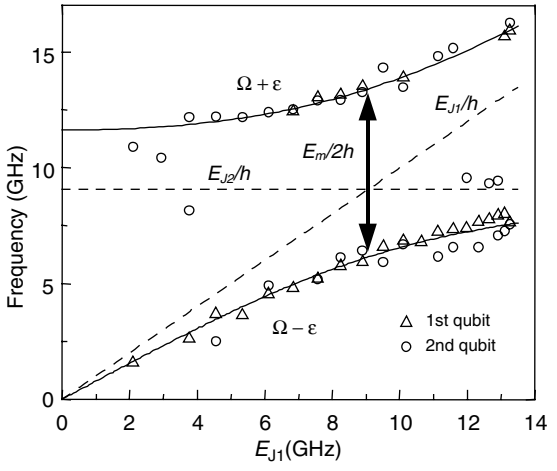

Fig. 7. E_{J1} dependence of the spectrum components of Fig. 6. Solid lines: dependence of $\Omega + \varepsilon$ and $\Omega - \varepsilon$ obtained from Eq. (6) using $E_{J2} = 9.1$ GHz and $E_m = 14.5$ GHz and varying E_{J1} from zero to its maximum value of 13.4 GHz. Dashed lines: dependence of the oscillation frequencies of both qubits in the case of zero coupling ($E_m = 0$).

($E_m = 0$), the single peaks in each qubit would follow dashed lines with an intersection at $E_{J1} = E_{J2}$. The introduced coupling modifies this dependence by creating a gap and shifting the frequencies to higher and lower values, the spacing between the two branches being equal to $E_m/2h$ when $E_{J1} = E_{J2}$. We compare the observed dependence with the prediction of Eq. (4) given by solid lines and find a remarkable agreement.

5. Entanglement of two qubits

The observed quantum coherent dynamics of coupled qubits in the vicinity of the double-degeneracy point X in Fig. 2 (in particular, double-frequency structure of the probability oscillations in both qubits and frequency "repulsion" at $E_{J1} \approx E_{J2}$—see Figs. 6 and 7) is a clear evidence for the interaction of two qubits. The fact that the two qubits interact, in turn, implies that they become entangled during the course of coupled oscillations although direct measurement of the degree of entanglement was not possible. We have done numerical simulations of the entanglement evolution using different measures for the amount of entanglement: negativity, concurrence and entropy of formation [24]. Here, we calculate analytically the amount of entanglement using a standard expression for the case of pure states [25] using entropy as a measure of the amount of entanglement. Using Hamiltonian (2) we calculated the time evolution of the entropy of entanglement for an ideal (rectangular) pulse shape:

$$E = 1 - \frac{1}{2\log 2}\left[\left(1-\sqrt{1-q}\right)\log\left(1-\sqrt{1-q}\right) + \left(1+\sqrt{1-q}\right)\log\left(1+\sqrt{1-q}\right)\right], \quad (6)$$

where

$$q = \frac{v^2}{\Omega^2}\sin^2\Omega t + \frac{v^2}{\varepsilon^2}\sin^2\varepsilon t - \frac{2v^4}{\Omega^2\varepsilon^2}\sin^2\Omega t\sin^2\varepsilon t - \frac{\Delta^2 v^2}{\Omega^4}\sin^4\Omega t - \frac{\delta^2 v^2}{\varepsilon^4}\sin^4\varepsilon t - \frac{v^2}{2\Omega\varepsilon}\sin 2\Omega t\sin 2\varepsilon t. \quad (7)$$

Here, $v = E_m/4\hbar$, $\Delta = (E_{J1} + E_{J2})/2\hbar$, $\delta = (E_{J2} - E_{J1})/2\hbar$ and Ω and ε were introduced in Eq. (4).

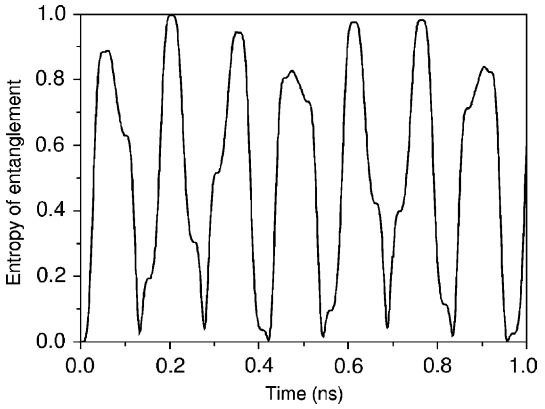

Fig. 8. Entropy of entanglement E evolution as described by Eq. (6).

E as a function of time for equal Josephson energies $E_{J1} = E_{J2} = 9.1$ GHz is shown in Fig. 8. This dependence coincides with numerically calculated entropy of formation as expected for pure bipartite systems. It has an oscillatory behavior and reaches unity at about 0.2 ns. This means that the two qubits become maximally entangled at this instance. Our numerical simulations show that the amount of entanglement does not decrease significantly when a realistic pulse shape is taken into account [26].

In conclusion, we were able to manipulate quantum states of two-coupled Josephson charge qubits using a common pulse gate and have observed time-domain oscillations with a clear evidence for interaction between the qubits. One of the next major steps towards building a Josephson junction quantum computer prototype will be the demonstration of controllable coupling between the qubits. A simple scheme for making controllable coupling between charge qubits has been proposed recently [27]. The hardest hurdle to overcome, however, is the short decoherence time that, in our case, is determined by energy relaxation [28].

Acknowledgements

We thank B.L. Altshuler, X. Hu, H. Im, S. Ishizaka, S. Lloyd, T. Sakamoto and J.Q. You for

fruitful discussions. D.V.A. was supported by the AFORS and by the NSA and ARDA under the ARO contract. T.T. and F.N. were supported in part by the National Security Agency (NSA) and Advanced Research and Development Activity (ARDA) under Air Force Office of Scientific Research (AFOSR) contract number F49620-02-1-0334; and also supported by the US National Science Foundation Grant No. EIA-0130383.

References

[1] M.A. Nielsen, I.L. Chuang, Quantum Computation and Quantum Information, Cambridge University Press, Cambridge, 2000.
[2] R.G. Clark (Ed.), Experimental Implementation of Quantum Computation, Rinton Press, Princeton, 2001.
[3] D.V. Averin, Fortschr. Phys. 48 (2000) 1055.
[4] Y. Makhlin, G. Schön, A. Shnirman, Rev. Mod. Phys. 73 (2001) 357.
[5] Y. Nakamura, Yu.A. Pashkin, J.S. Tsai, Nature 398 (1999) 786.
[6] D. Vion, A. Aasime, A. Cottet, P. Joyez, H. Pothier, C. Urbina, D. Esteve, M.H. Devoret, Science 296 (2002) 886.
[7] T. Duty, D. Gunnarsson, K. Bladh, P. Delsing, Phys. Rev. B 69 (2004) 140503.
[8] I. Chiorescu, Y. Nakamura, C.J.P.M. Harmans, J.E. Mooij, Science 299 (2003) 1869.
[9] Y. Yu, S. Han, X. Chu, S.-I. Chu, Z. Wang, Science 296 (2002) 889.
[10] J.M. Martinis, S. Nam, J. Aumentado, C. Urbina, Phys. Rev. Lett. 89 (2002) 117901.
[11] T. Hayashi, T. Fujisawa, H.D. Cheong, Y.H. Jeong, Y. Hirayama, Phys. Rev. Lett. 91 (2003) 226804.
[12] O. Astafiev, Yu.A. Pashkin, T. Yamamoto, Y. Nakamura, J.S. Tsai, Phys. Rev. B 69 (2004) 180507(R).
[13] Yu.A. Pashkin, T. Yamamoto, O. Astafiev, Y. Nakamura, D.V. Averin, J.S. Tsai, Nature 421 (2003) 823.
[14] A.J. Berkley, H. Xu, R.C. Ramos, M.A. Gubrud, F.W. Strauch, P.R. Johnson, J.R. Anderson, A.J. Dragd, C.J. Lobb, F.C. Wellstood, Science 300 (2003) 1548.
[15] J.B. Majer, F.G. Paauw, A.C.J. ter Haar, C.J.P.M. Harmans, J.E. Mooij, Phys. Rev. Lett. 94 (2005) 090501.
[16] M. Büttiker, Phys. Rev. B 36 (1987) 3548.
[17] V. Bouchiat, D. Vion, P. Joyez, D. Esteve, M.H. Devoret, Phys. Scr. T 76 (1998) 165.
[18] Y. Nakamura, C.D. Chen, J.S. Tsai, Phys. Rev. Lett. 79 (1997) 2328.
[19] D.V. Averin, A.B. Zorin, K.K. Likharev, ZhETP 88 (1985) 692 [Sov. Phys. JETP 61 (1985) 407].
[20] H. Pothier, P. Lafarge, C. Urbina, D. Esteve, M.H. Devoret, Europhys. Lett. 17 (1992) 249.
[21] T. Yamamoto, Yu.A. Pashkin, O. Astafiev, Y. Nakamura, J.S. Tsai, Nature 425 (2003) 941.
[22] T.A. Fulton, P.A. Gammel, D.J. Bishop, L.N. Dunkleberger, G.J. Dolan, Phys. Rev. Lett. 63 (1989) 1307.
[23] K. Rabenstein, D.V. Averin, Turk. J. Phys. 27 (2003) 313. Available from: <cond-mat/0310193>.
[24] Yu.A. Pashkin, T. Tilma, D.V. Averin, O. Astafiev, T. Yamamoto, Y. Nakamura, F. Nori, J.S. Tsai, Int. J. Quantum Inform. 1 (2003) 421.
[25] C.H. Bennett, H.J. Bernstein, S. Popescu, B. Schumacher, Phys. Rev. A 53 (1996) 2046.
[26] T. Tilma et al., unpublished.
[27] D.V. Averin, C. Bruder, Phys. Rev. Lett. 91 (2003) 057003.
[28] O. Astafiev, Yu.A. Pashkin, T. Yamamoto, Y. Nakamura, J.S. Tsai, Phys. Rev. Lett. 93 (2004) 267007.